Entropy-Patch-Choked-Nozzle Interaction: Quasi-Steady-Modeling-Regime Limits Probed

Kowalski, K.; Hulshoff, S.J.; Ströer, P. ; Withag, Jan; Genot, A. ; Morgans, A. S. ; Bake, F.; Venner, K. ; Sanders, Martinus P.J.; Hirschberg, L.

DOI
10.2514/6.2024-3113

Publication date
2024

Document Version
Final published version

Published in
30th AIAA/CEAS Aeroacoustics Conference (2024)

Aeroacoustics Conferences
June 4-7, 2024, Rome, Italy
30th AIAA/CEAS Aeroacoustics Conference (2024)

10.2514/6.2024-3113

Entropy-patch choked-nozzle interaction: quasi-steady-modeling-regime limits probed

K. Kowalski *
University of Twente, 7522 NB Enschede, The Netherlands

S. J. Hulshoff†
Delft University of Technology, 2629HS Delft, The Netherlands

P. Ströer‡
University of Twente, 7522 NB Enschede, The Netherlands

J. Withag§
University of Twente, 7522 NB Enschede, The Netherlands

A. Genot ¶
ONERA, 31000 Toulouse, France

A. S. Morgans‖
Imperial College London, London SW7 1AY, UK

F. Bake**
BAM, 12205 Berlin, Germany

K. Venner††
University of Twente, 7522 NB Enschede, The Netherlands

M. P. J. Sanders‡‡
University of Twente, 7522 NB Enschede, The Netherlands

L. Hirschberg§§
University of Twente, 7522 NB Enschede, The Netherlands

Indirect combustion noise due to the interaction of flow inhomogeneities with a choked

*MSc student, University of Twente, Thermal and Fluid Engineering Department, Engineering Fluid Dynamics, University of Twente, Drienerlolaan 5, Enschede, 7522 NB, The Netherlands.

†Assistant Professor, Faculty of Aerospace Engineering, Delft University of Technology, Kluyverweg 1, 2629HS Delft, The Netherlands.

‡Assistant Professor, University of Twente, Thermal and Fluid Engineering Department, Engineering Fluid Dynamics, University of Twente, Drienerlolaan 5, Enschede, 7522 NB, Netherlands.

§Lecturer, University of Twente, Thermal and Fluid Engineering Department, Engineering Fluid Dynamics, University of Twente, Drienerlolaan 5, Enschede, 7522 NB, Netherlands.

¶Research Scientist, Multi-Physics for Energetics Department, ONERA (The French Aerospace Lab), Université de Toulouse, 31000 Toulouse, France

‖Professor of Thermofluids, Imperial College London, Department of Mechanical Engineering, South Kensington Campus, London SW7 2AZ, UK.

**Division for Acoustic and Electromagnetic Methods, Department of Non-destructive Testing, Bundesanstalt für Materialforschung und -prüfung (BAM), Unter den Eichen 87, 12205 Berlin, Germany, AIAA Associate Fellow.

††Full Professor, University of Twente, Thermal and Fluid Engineering Department, Engineering Fluid Dynamics, University of Twente, Drienerlolaan 5, Enschede, 7522 NB, Netherlands,

‡‡Assistant Professor, University of Twente, Thermal and Fluid Engineering Department, Engineering Fluid Dynamics, University of Twente, Drienerlolaan 5, Enschede, 7522 NB, Netherlands.

§§Assistant Professor, University of Twente, Thermal and Fluid Engineering Department, Engineering Fluid Dynamics, University of Twente, Drienerlolaan 5, Enschede, 7522 NB, Netherlands, AIAA Senior Member.

combustion-chamber exit is an important cause of combustion instability in solid rocket motors. Moreover, it is believed to be an issue in electrical-power generation turbines and aero-engines. If these flow inhomogeneities are essentially characterized by the fluid having a locally appreciably-different thermodynamic state, the acoustic response engendered by its interaction with the combustion-chamber exit is commonly referred to as entropy noise. In this paper, dedicated numerical-simulation results of entropy-patch choked-nozzle interactions are presented. Two types of entropy patches were considered: rectangular slugs and circular spots. Moreover, analytical-model-based analysis, of said simulation results, is presented. Based on said analysis, the authors posit the existence of three modeling regimes: the quasi-steady-modeling regime, the blended-physical-effects regime, and the inertial-modeling regime.

I. Introduction

Engineering systems employing turbulent combustion usually have high levels of noise production, due both to direct and indirect combustion-noise sources. Direct sources, due to unsteady gas expansion in flames, have been widely studied [1–3]. Indirect sources include entropy noise and vorticity noise. In particular, both entropy patches and vortices produce sound waves as they exit the combustion chamber through a nozzle or turbine. Some of these sound waves are radiated into the environment, and some are reflected back into the combustion chamber. The latter can produce new entropy patches and vortices, which in turn produce new sound waves as they exit the combustion chamber. Under unfavorable circumstances, this results in a feedback loop which promotes combustion instability or self-sustained pressure pulsations. Thermo-acoustic combustion-chamber instabilities driven by indirect combustion noise are a potential issue in aero-engines and electrical-power generation turbines [2, 3]. In large solid rocket motors: vorticity-noise-driven self-sustained pressure pulsations are an established issue [4–9].

In order to cultivate fundamental understanding of complex phenomena such as indirect combustion noise, it is standard practice to perform order-reduction by designing experiments in which only one effect is dominant—or on occasion, when the former has been done, in which: only a couple effects are dominant [6, 10–17]. A prime example of this approach are Anthoine's et al. [6] cold-gas—viz. without combustion—scale-model experiments, which were used to investigate self-sustained pressure pulsations in solid rocket motors. Indeed, these demonstrated the importance of the integrated nozzle's nozzle-cavity volume on indirect noise produced by essentially nonlinear azimuthal-vortex-nozzle (or ring-vortex-nozzle) interaction. Other examples are Bake's et al. [10] canonical entropy-noise experiment, De Domenico's et al. experiment [14], Noiray & Wellemann's experiment [15], and Hirschberg's et al. entropy and normal-component-vorticity noise experiments [13, 16, 17]. Moreover, the practice of studying indirect combustion-noise sources in isolation has also been successfully used for the development of analytical and numerical indirect combustion-noise models [9, 18–21].

Of the two indirect combustion-noise sources, entropy noise has been the most widely studied, as evidenced by the high number of citations of two seminal articles by Marble & Candel [18] and Ffowcs Williams & Howe [19]. Marble & Candel's one-dimensional (1D) modeling approach [18, 19], based on the notion of plane entropy-wave interaction with a nozzle, appears to be the most widely applied. In contrast, Ffowcs Williams & Howe's method considers: three-dimensional patches of the fluid—with relative-excess density—convected by the flow [19].

Ffowcs Williams & Howe seem to have argued that "*to elicit in detail the physical mechanisms responsible for the generation of sound*" [19] the inclusion of acceleration/unsteadiness is an ineluctable ingredient for a model. Whereas, Marble & Candel astutely pointed out: "*When the scale of the disturbance impinging upon the nozzle is large in comparison with the nozzle length ... the response of the nozzle is well approximated by a quasi-steady analysis. Though limited in the range of frequency over which it is applicable, the results which follow from this approximation are simple and extremely useful. The idea is simply that, to disturbances of very long wave length* [*sic*]*, the nozzle appears as a discontinuity in the state of the medium supporting the propagation; the state gradients ... become discontinuities. The nozzle then provides matching conditions, between uniform upstream and downstream states, which may be derived from conservation laws and the geometric description of the nozzle.*"

For the case of choked-nozzle-flow experiments, Hirschberg et al. [17] used Marble & Candel's above-quoted observation, to formulate a bare-bones—essentially quasi-steady—model. Said model was validated by comparison with Leyko's et al. [20] simulation results [17]. Moreover, Hirschberg et al. [17] pointed out that in the cases where quasi-steady modeling is applicable: sound production is due to a temporary axial mass-flow rate change caused by the passage of an entropy patch through the nozzle throat.

Given that Ffowcs Williams & Howe's method is not limited to one-dimensionality, it allows for the investigation of the entropy patch's shape on sound production. Using their approach, Ffowcs Williams & Howe investigated the influence of the entropy patch's size on sound generation, which they termed "*acoustic bremsstrahlung*" or "*bremsstrahlung*" [19]. In particular, they used their model to compare sound generation of a duct-sized entropy "*slug*" to a much smaller spherical "*pellet*," as these pass through a duct contraction or a nozzle [19]. One should note that Ffowcs Williams & Howe only considered low-Mach-number flow; viz., they did not consider choked-nozzle flows.

In the presently-reported study, inspired by Ffowcs Williams & Howe's work, but with a focus on choked-nozzle-flow cases, the authors investigated the influence of an entropy patch's shape and more importantly its size on: the upstream-traveling acoustic response due to the passage of an entropy patch. In particular, they sought to identify the limits of the quasi-steady-modeling regime and elucidate the role of the entropy patch's size and shape.

II. Theory

A. Quasi-steady one-dimensional model

In the following: a model for the upstream observed acoustic pressure response p'_{ob}, due to the interaction of an entropy patch of relative excess density $\rho_e/\bar{\rho} \equiv (\rho - \bar{\rho})/\bar{\rho}$ with a choked nozzle is derived. Here ρ and $\bar{\rho}$ are the density with and without the presence of an entropy patch, respectively. The (unperturbed) base flow carrying the entropy patch is taken to be steady. One assumes that $\rho_e/\bar{\rho}$ is small enough, such that the entropy patch is carried by the base flow without affecting it. Upstream from the nozzle, the flow is taken to be one-dimensional (1D); viz., the local flow variables vary only in the axial direction and are taken to be locally uniform over a cross section at any particular axial position x. Furthermore, it is assumed that the interaction-time scale of the entropy patch with the nozzle is significantly larger than the travel time of a material element through the nozzle.

The local base flow Mach number M is defined as:

$$M \equiv \frac{u}{c} \tag{1}$$

where u and c are the local axial velocity and speed of sound, respectively. For a choked nozzle M at the nozzle inlet is fixed by its geometry. Hence, for the perturbations of the base flow velocity u' and speed of sound c', at the nozzle inlet one has:

$$\frac{c'}{c} = \frac{u'}{u} \tag{2}$$

Assuming formation of an entropy patch of relative excess density $\rho_e/\bar{\rho}$ at constant pressure (isobaric process), for a perfect gas, one finds

$$\frac{\rho_e}{\bar{\rho}} = -2\frac{c'}{c} \tag{3}$$

and after some algebra

$$u' = -\frac{1}{2}\left(\frac{\rho_e}{\bar{\rho}}\right) Mc \tag{4}$$

Taking the positive flow direction to be from upstream to downstream, and assuming an infinitely long uniform duct upstream from the nozzle, the acoustic pressure perturbation p'_u observed upstream is

$$p'_u = p^-_u = -\rho c u' = \frac{1}{2}\left(\frac{\rho_e}{\bar{\rho}}\right)\gamma p M \tag{5}$$

where $p = \rho c^2/\gamma$ is the static pressure of the flow at the nozzle inlet. This result will be referred to as the quasi-steady

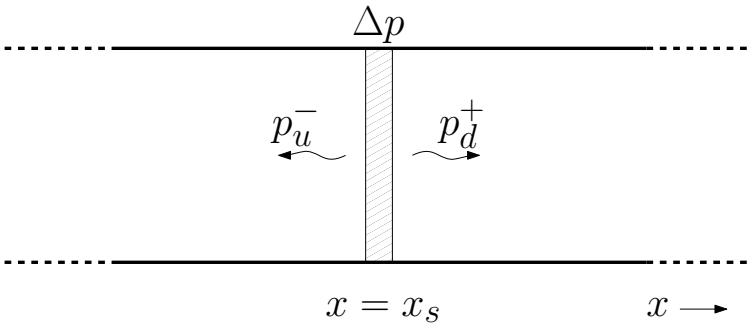

Fig. 1 Fluctuating pressure discontinuity Δp at $x = x_s$, in a uniform 1D ducted flow. Plane acoustic pressure waves: p_u^- and p_d^+ emanate from Δp in the up- and downstream direction, respectively.

1D model or quasi-steady model, in the remainder of the text.

B. Quasi-one-dimensional point-mass model

Consider a sound source in the form of a fluctuating pressure discontinuity Δp at position $x = x_s$ in a duct of uniform cross-section with a uniform 1D flow with Mach number M. The amplitudes of plane acoustic pressure $p^\pm$ and density waves $\rho^\pm$, are related as follows:

$$p^\pm = c^2 \rho^\pm \tag{6}$$

where the superscripts + or − indicate a plane wave traveling in the positive or negative direction with respect to the uniform 1D base flow. For the acoustic velocity waves $u^\pm$, one has

$$u^\pm = \pm \frac{p^\pm}{\rho c}. \tag{7}$$

As sketched in Fig. 1, two plane waves are generated on either side of the pressure discontinuity: p_u^+ and p_d^-, where the subscripts u and d stand for up- and downstream, respectively. Assuming anechoic duct terminations, one can express Δp in terms of the acoustic pressure waves emanating from it:

$$\Delta p = p_d^+ - p_u^-. \tag{8}$$

Across the pressure discontinuity the mass flux ρu is conserved, so that

$$\rho_d^+ u + \rho u_d^+ = \rho_u^- u + \rho u_u^- \tag{9}$$

Using Eqs. (6) and (7), one finds the following expressions:

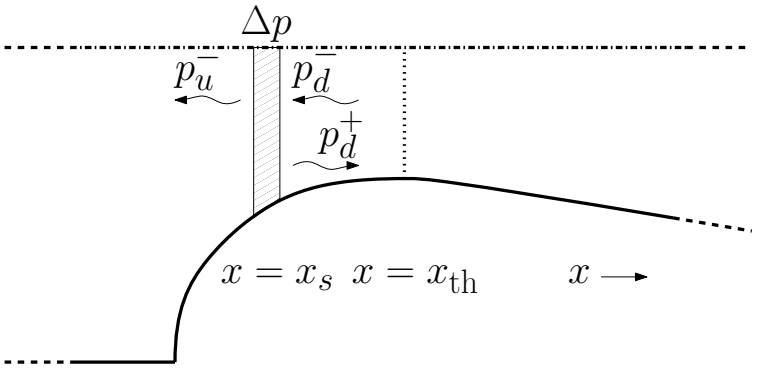

Fig. 2 Acoustic pressure waves emanating from a fluctuating pressure discontinuity Δp located at $x = x_s$ in the converging part of a choked nozzle. As the nozzle is choked and the flow is 1D, one has sonic line at $x = x_{\mathrm{th}}$, viz., in the throat.

$$p_d^+ = \frac{1 - M_s}{2}\Delta p \tag{10}$$

$$p_u^- = -\frac{1 + M_s}{2}\Delta p \tag{11}$$

where M_s is the Mach number at the sound source position x_s.

Moving forward it will be assumed that the above result obtained for a uniform cross-section duct can be applied in the subsonic parts of a choked nozzle with varying cross-sectional area $A = A(x)$. In this quasi-1D approximation A varies slowly in the flow direction, viz.,

$$\frac{L_{\mathrm{nozzle}}}{\sqrt{A}}\frac{\mathrm{d}A}{\mathrm{d}x} << 1. \tag{12}$$

where L_{nozzle} is the length of the nozzle.

The acoustic wave p_d^+ is partially reflected by the nozzle. Assuming quasi-steady behavior for this process, one can apply Eq. (2) to an adiabatic pressure perturbation and after some algebra one finds:

$$\frac{p_d^+ - p_d^-}{\rho c u} = \frac{\gamma - 1}{2\gamma}\frac{p_d^+ + p_d^-}{\rho c^2} \tag{13}$$

which, when solving for the reflection coefficient $R \equiv p_d^-/p_d^+$, yields

$$R = \frac{1 - \frac{\gamma-1}{2}M_s}{1 + \frac{\gamma-1}{2}M_s}. \tag{14}$$

The pressure fluctuation p_u' moving upstream from Δp is

$$p'_u = p^-_u + R p^+_d. \tag{15}$$

Using Eqs. (10) and (11), one finds

$$p'_u = -\frac{\Delta p}{2}\left((1+M_s) - R\,(1-M_s)\right). \tag{16}$$

where M_s is the Mach number at $x = x_s$. The acoustic power emitted upstream is

$$|\Phi^-_s| = \frac{A_s}{\rho_s c_s}|p'_u|^2\,(1-M_s)^2\,. \tag{17}$$

At an upstream (observer) position $x = x_{\mathrm{ob}}$, the observed acoustic-power flow $|\Phi^-_{\mathrm{ob}}|$, is

$$|\Phi^-_{\mathrm{ob}}| = \frac{A_{\mathrm{ob}}}{\rho_{\mathrm{ob}} c_{\mathrm{ob}}}|p'_{\mathrm{ob}}|^2\,(1-M_{\mathrm{ob}})^2\,. \tag{18}$$

Taking the energy transport to $x = x_{\mathrm{ob}}$ to be lossless, viz., that $|\Phi^-_{\mathrm{ob}}| = |\Phi^-_s|$, one finds

$$|p'_{\mathrm{ob}}| = \sqrt{\frac{\rho_{\mathrm{ob}} c_{\mathrm{ob}}}{\rho_s c_s}\frac{A_s}{A_{\mathrm{ob}}}}\left((1+M_s) - R\,(1-M_s)\right)\left(\frac{1-M_s}{1-M_{\mathrm{ob}}}\right)\frac{\Delta p}{2} \tag{19}$$

Assuming an entropy "point particle," the excess mass is

$$m_e \equiv \int_{V_e} \rho_e \mathrm{d}^3 x, \tag{20}$$

where the volume integral is taken over the volume of the entropy patch V_e. By virtue of Newton's second law, one has that the walls of the nozzle have to exert a force F_x on the flow to provide the acceleration of the "point particle"

$$F_x = m_e\left(u\frac{\mathrm{d}u}{\mathrm{d}x}\right) \tag{21}$$

From Curle's [22] analogy or Gutin's [23] principle, one knows that an unsteady force of a wall on the fluid is a source of sound. In this case, represents this dipolar sound source as the pressure discontinuity:

$$\Delta p = \frac{F_x}{A_s} \tag{22}$$

Substituting Eq. (22) in Eq. (19), yields

$$|p'_{\mathrm{ob}}| = \sqrt{\frac{\rho_{\mathrm{ob}} c_{\mathrm{ob}}}{\rho_s c_s}\frac{1}{A_{\mathrm{ob}} A_s}}\left((1+M_s) - R\,(1-M_s)\right)\left(\frac{1-M_s}{1-M_{\mathrm{ob}}}\right)\frac{m_e}{2}\left(u\frac{\mathrm{d}u}{\mathrm{d}x}\right). \tag{23}$$

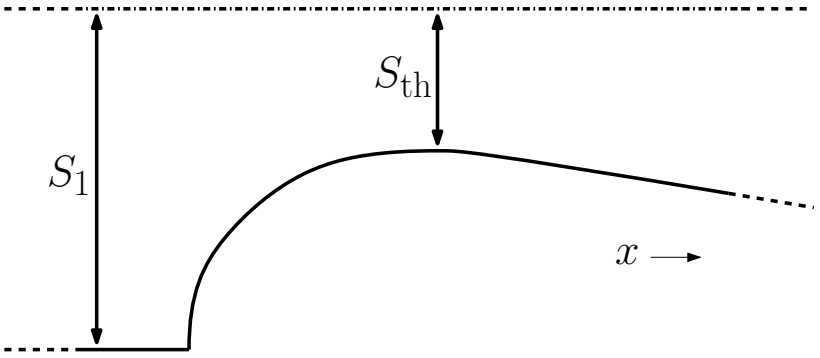

Fig. 3 S_1 **and** S_{th} **are the upstream half-duct height and the half height in the throat, respectively.**

Using Bernoulli's principle and isentropic perfect gas relations, one finds

$$\sqrt{\frac{\rho_{\mathrm{ob}} c_{\mathrm{ob}}}{\rho_s c_s}} = \left(\frac{1 + \frac{\gamma-1}{2} M_s^2}{1 + \frac{\gamma-1}{2} M_{\mathrm{ob}}^2} \right)^{\frac{\gamma+1}{4(\gamma-1)}} \tag{24}$$

and

$$\frac{A_s}{A_{\mathrm{th}}} = \frac{1}{M_s} \left(1 + \frac{\gamma-1}{\gamma+1} (M_s^2 - 1) \right)^{\frac{\gamma+1}{2(\gamma-1)}} \tag{25}$$

where $A_{\mathrm{th}} = 4 S_1 S_{\mathrm{th}}$ with S_1 and S_{th} the upstream half-duct height and the half height in the throat as defined in Fig. 3.

The convective acceleration, $u\mathrm{d}u/\mathrm{d}x$ in Eqs. (21) and (22), can be estimated from two-dimensional (plane) numerical simulations of the stationary base flow (Appendix A). When such estimations are used in Eq. (22) the results will be said to have been obtained using the hybrid point-mass model or hybrid model.

In Fig. 4, results of this hybrid point-mass model are shown. Speciffically, the dimensionless upstream observed acoustic response $|p'_{\mathrm{ob}}| S_1^3 / (m_e U_1^2)$ is shown as a function of the dimensionless source position $(x_s - x_{\mathrm{th}})/S_1$ in the convergent part of the nozzle upstream from the throat position x_{th}. The hybrid point-mass model results demonstrate that $|p'_{\mathrm{ob}}|$ is primarily generated close to the throat, at around $(x_s - x_{\mathrm{th}})/S_1 = -0.1$.

III. Numerical simulations: methodology

Systematic studies of entropy-spot-choked-nozzle interaction were carried out using Hulshoff's state-of-the-art two-dimensional (plane) Euler Internal Aeroacoustics code (EIA) [24–26], which solves the compressible frictionless governing (Euler) equations:

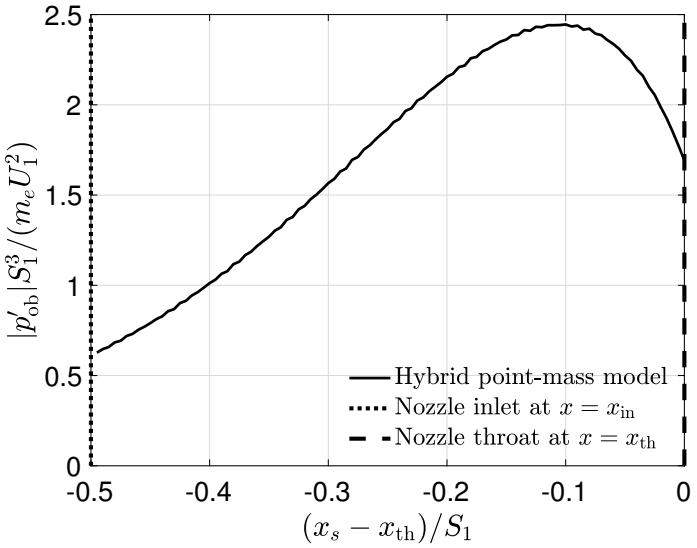

Fig. 4 Dimensionless upstream observed acoustic response $|p'_{\rm ob}|S_1^3/(m_e U_1^2)$ as a function of the dimensionless source position $(x_s - x_{\rm th})/S_1$ in the convergent part of the nozzle. The finely dotted and dashed vertical lines indicate the position of the nozzle inlet and throat, respectively.

$$\frac{\partial \rho}{\partial t} + \nabla \cdot (\rho \mathbf{u}) = 0 \tag{26}$$

$$\frac{\partial \rho \mathbf{u}}{\partial t} + \nabla \cdot (\rho \mathbf{u}\mathbf{u} + p\mathbf{1}) = \rho \mathbf{F}_E \tag{27}$$

$$\frac{\partial E_T}{\partial t} + \nabla \cdot ((E_T + p)\mathbf{u}) = Q_E \tag{28}$$

where $E_T = \rho(e + |\mathbf{u}|^2/2)$ is the total energy density, $\rho \mathbf{F}_E$ is an external momentum source density and Q_E is an external energy source. The energy source term Q_E was used to generate entropy patches. In conjunction with the heat capacity ratio $\gamma = 1.4$, the ideal gas law was used as an equation of state. The authors note that the external momentum source $\mathbf{F}_E$ can be used to generate vortices, as was done by Hulshoff et al. [25] and Hirschberg et al. [7–9]. Moreover, the methodology applied here is essentially the same as was reported by Hirschberg et al. [8, 27]; viz.:

1) Computational meshes were generated.
2) A steady choked-nozzle base flow was established.
3) Unsteady entropy-spot-choked-nozzle-interaction simulations were performed, with the steady choked-nozzle base flow as an initial condition (IC). Namely, entropy patches (circular spots or rectangular slugs) were generated atop the IC.

In this section, the above steps are briefly expanded upon in §III.A, §III.B, and III.C, respectively.

Fig. 5 Geometry of the computational domain, with $S_1/S_{\text{th}} = 3$, used for the presently-presented study.

A. Computational mesh generation and information re numerical accuracy

In this subsection, details regarding mesh generation for the convergent-divergent-nozzle configuration used for the present study are provided. In Fig. 5, the computational domain's geometry for the configuration is shown. The domain consists, from left to right, of: blocks 1 (green), 2 (red), 3 (yellow) and 4 (blue). Blocks 3 and 4 form a convergent-divergent nozzle with a contraction ratio: $S_1/S_{\text{th}} = 3$ (where $2S_1$ is upstream channel height and $2S_{\text{th}}$ is the height at the nozzle throat), which for a choked-nozzle flows, corresponds to an upstream Mach number of $M = 0.20$.

To perform entropy-patch choked-nozzle interaction simulations: entropy patches were generated on block 1, in which it was ensured that cells produced during mesh-generation: had a square shape—to minimize small asymmetries. The entropy patches were generated by application of a non-uniform external energy source Q_E (consult §III.C.2 for details) on this block. Block 2 served as a transition from the generation block to block 3. This was done to gradually change the mesh geometry whilst keeping the cells as square as possible. Block 3 contained the contraction part of the convergent-divergent nozzle (its inlet). The lower wall of the contraction in block 3 was generated using the Henrici transformation [28] for the analytical model (with contraction length $L_{\text{contraction}}/S_1 = 1/2$, for more info the reader is invited to consult Ref. [29]). Finally, one had, downstream from the contraction, block 4: the diverging part of said convergent-divergent nozzle (diffusor).

The number of points on each mesh was chosen to have a sufficient number of points per spot radius R_s or half slug width $W_s/2$ of the entropy patch to ensure grid-independent solutions. The spatial discretization used for the entropy-patch-nozzle-interaction simulations was based on a second-order total-variation-diminishing (TVD) Roe approximate Riemann solver with a van Leer limiter [30]. A five-stage Runge-Kutta time marching method was used for time integration. Using three meshes with 36, 54 and 81 points per $R_s/S_1 = 0.3$, Hirschberg et al. [7–9] determined: the estimated order-of-accuracy [31] to be 1.8 with a discretization error of approximately 1%. Ergo, for the purposes of the presently-reported study meshes: were generated with at least 36 points per length-scale of the entropy patch used to perform unsteady simulations.

The same number of points on the left-hand (inlet) boundary of block 1 were used on the right-hand boundary of block 1 as well as the left- and right-hand boundaries of block 2. Furthermore, the number of points on the upper and

lower channel walls of block 1 were chosen, such that the resulting cells were to a satisfactory degree square. The change of a cell-surface area from cell to cell was kept as small as possible. Moreover, the number of points on the sides of the individual blocks was kept divisible by four to allow a three-level explicit multi-grid (EMG) method to be used to establish the base flow [24]. The initialization procedure of the choked-nozzle base flow is briefly described in the following subsection.

B. Establishment of a steady choked-nozzle base flow

Before unsteady entropy-patch choked-nozzle interaction could be studied, a steady choked-nozzle base flow had to be established on the computational domain (Fig. 5). Subsequently, this flow was used as an initial condition, atop which entropy patches were generated to investigate: sound production due to entropy-patch choked-nozzle interaction. Generation of entropy patches and the applied boundary conditions for the unsteady simulations are discussed in §III.C.2. In this subsection, the establishment of the base flow is described.

The boundary conditions [24], which were imposed to establish said base flow where:

- A "usoft" boundary condition on the upstream wall (on the left-hand-side of Fig. 5). This boundary condition imposes:
  - a desired normal time averaged inflow velocity U_{des},
  - the local sound speed (which was set to one),
  - the local density (which is set to one).
- Wall boundary conditions on the lower and upper walls of the channel (vanishing normal velocity).
- Connection boundary conditions on all the interfaces connecting the constituent blocks of the channel.
- A non-reflective boundary condition on the downstream domain boundary.

To determine the upstream inlet velocity, U_{des}, for a choked nozzle, the isentropic quasi-one-dimensional relation:

$$S_{\text{th}}/S_1 = M \left(\frac{\gamma + 1}{2(1 + \frac{\gamma-1}{2} M^2)} \right)^{\frac{\gamma+1}{2(\gamma-1)}} \tag{29}$$

was used [32]. The equation was solved numerically to determine: which inlet Mach number needs to be imposed to ensure the establishment of a steady choked-nozzle base flow.

All the individual blocks of the mesh were assigned initial values of: the density, ρ_{initial}, the velocity $\mathbf{u}_{\text{initial}} = (u, v)$ and the pressure p_{initial}. On blocks 1, 2 and 3 the following values were imposed: $\rho_{\text{initial}} = 1$, $\mathbf{u}_{\text{initial}} = (U_{\text{des}}, 0)$ and $p_{\text{initial}} = c^2 \rho_{\text{initial}}/\gamma$, where $\gamma = 1.4$ is the heat capacity for diatomic gas and c is the sound speed. c was set to 1 $\text{m} \cdot \text{s}^{-1}$ in the upstream blocks 1 and 2, by means of the "usoft" boundary condition [24]. On the downstream section of the mesh (block 4): $\rho_{\text{initial}} = 1$, $\mathbf{u}_{\text{initial}} = (1, 0)$ and $p_{\text{initial}} = c^2 \rho_{\text{initial}}/(2\gamma)$ were imposed. Consequently, the pressure in block 4 was lower by a factor two compared to the upstream blocks 1, 2, and 3. This ensured that no shock-wave was formed

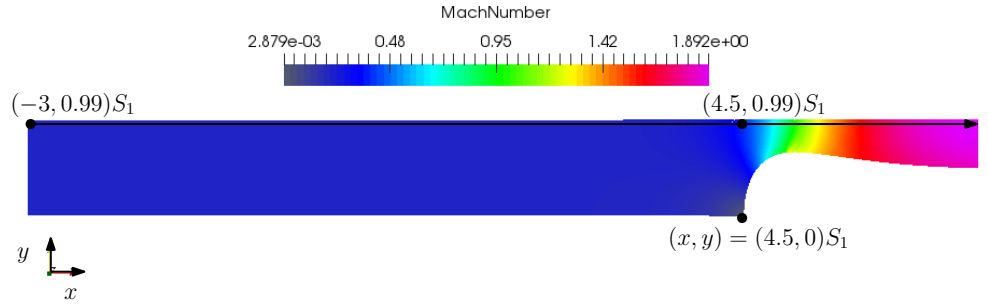

(a)

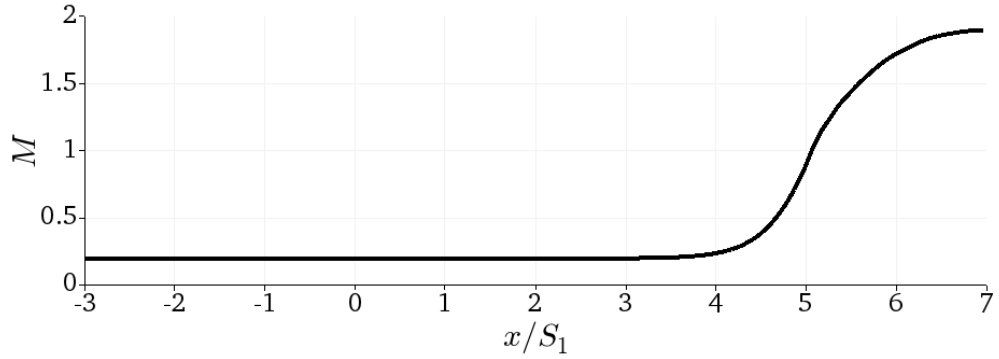

(b)

Fig. 6 Steady choked-nozzle base flow established for $S_1/S_{\text{th}} = 3$.

downstream from the sonic line in the contraction, and that the ultimately-reached flow remained supersonic in block 4.

The initial condition base flow (IC) to be used for unsteady entropy-patch choked-nozzle interaction simulations was established using a three-level explicit multi-grid relaxation scheme. Spatial integration was performed using a second-order total-variation-diminishing (TVD) Roe approximate Riemann solver with a van Leer limiter [24, 30]. Time marching was done using: a (5,2) Runge-Kutta scheme with a Courant number $Co = 2$ [24]. The simulation was run for more than a hundred-thousand time steps, with the aim of eliminating all transients. The resulting IC for the contraction ratio $S_1/S_{\text{th}} = 3$ and an upstream inlet Mach number $M = 0.20$ is shown in Fig. 6.

C. Entropy-patch-nozzle-interaction simulations: boundary conditions and entropy-patch generation

In this subsection, the boundary conditions applied to carry out: unsteady entropy-patch choked-nozzle interaction simulations are reported (§III.C.1). Moreover, entropy-patch generation is succinctly covered in §III.C.2.

1. Boundary conditions, pressure-probe positions and emission time

The boundary conditions [24] applied for the unsteady entropy-patch-nozzle-interaction simulations, were:

- An acoustically non-reflective condition on the upstream wall (left-hand-side boundary on Fig. 5)—it:

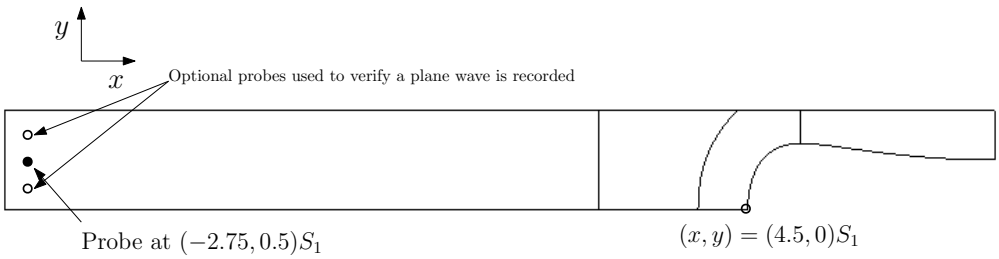

Fig. 7 Probe positions

  - mimics a connection to an infinite upstream channel,
  - maintains the local average inflow velocity, density and sound speed imposed by the base flow as an initial condition.
- A symmetry condition was applied on the dash-dotted boundary in Fig. 5.
- Connection boundary conditions on all the interfaces connecting the constituent blocks of the channel.
- Non-reflective boundary condition on the downstream end boundary (right-hand-side Fig. 5). The authors note: because a choked-nozzle flow was considered, the choice of outflow boundary condition was not critical (information cannot travel back upstream through a sonic line).
- Wall boundary conditions on the walls of the channel.

The acoustically non-reflective boundary conditions imposed on the upstream boundary of the computational domain allow one to record the upstream-traveling acoustic response due to entropy-patch-nozzle interaction, without: the interference of downstream-traveling spurious acoustic reflections. Indeed, if one had imposed boundary conditions which reflect acoustic waves, it would have significantly more difficult to separate the upstream-traveling acoustic wave due to entropy-patch-nozzle interaction (the quantity of interest) downstream traveling acoustic waves. The latter are due to reflections and engendered during the entropy-patch-generation phase. This methodology allows one to neatly separate the different events in time. Ergo, cogently separating the quantity of interest, in terms of time signal, from signals which are not pertinent.

To record the quantity of interest, the upstream acoustic response, p', a probe was placed at $\mathbf{x}_{\text{probe}} = (-2.75, 0.5)S_1$ close to the computational domain's upstream boundary (Fig. 7) to record: the pressure $p_{\text{probe}} = p_{\text{probe}}(t)$. The acoustic response was determined using $p' = p_{\text{probe}}(t) - p_{\text{probe}}(t_{\text{end}})$. The simulations were run for a time sufficiently long, to ensure that when $t = t_{\text{end}}$: one could assume that the flow field had returned to its stationary base-flow state. The acoustic response was determined to be a plane wave, by means of two additional probes, which were placed at $(-2.75, 0.52)S_1$ and $(-2.75, 0.75)S_1$ (indicated with the open circles in Fig. 7).

The travel time, t_t, the time the acoustic wave took to reach the probe coming from the nozzle, was estimated as follows:

(a) Fully-mature entropy slug generated with $W_s/(2S_1) = 1.0$

(b) Fully-mature entropy spot generated with $R_s/S_1 = 1.0$

(c) Fully-mature entropy slug generated with $W_s/(2S_1) = 3.0$

(d) Fully-mature entropy spot generated with $R_s/S_1 = 3.0$

Fig. 8 Fully-mature entropy patches.

$$t_t = \frac{|\mathbf{x}_{\text{probe}} - \mathbf{x}_{\text{th}}|}{c_1 - U_1} \tag{30}$$

where $|\mathbf{x}_{\text{probe}} - \mathbf{x}_{\text{th}}| = 7.25S_1$ is the distance from the nozzle inlet ($x_{\text{inlet}} = 4.5S_1$) to the probe ($x_{\text{probe}} = -2.75$). Using t_t, the retarded time is defined as follows:

$$t_r \equiv t - t_t \tag{31}$$

The upstream-recorded acoustic response signals, obtained from entropy-patch-nozzle-interaction simulations, will be presented as a function of t_r in §IV.

2. Entropy-patch generation

To generate a fully mature entropy patch—i.e., a slug or spot like the ones shown in Fig. 8—the energy-source term Q_E in Eq. 28 was used. The entropy patch was generated by means of localized energy injection around a point, which was convected with the base flow. The energy source Q_E was chosen to be the following a function of the user-set characteristic length of the to-be-generated entropy patch L_s—i.e., the spot radius R_s or half the slug width $W_s/2$.

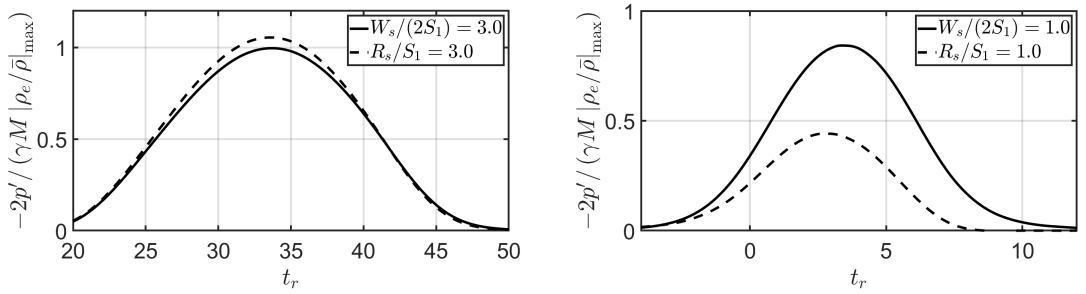

Fig. 9 The upstream acoustic response scaled by the quasi-steady-model prediction vs. retarded time, for four patch sizes: (a) $R_s/S_1 = 3.0$ and $W_s/(2S_1) = 3.0$ & (b) $R_s/S_1 = 1.0$ and $W_s/(2S_1) = 1.0$.

$$Q_E = \begin{cases} \frac{A_E}{2}\left(1 + \cos\left(\pi\frac{\zeta}{L_s}\right)\right) \text{ if } 0 \le \zeta \le L_s \\ 0 \text{ if } \zeta > L_s \end{cases} \tag{32}$$

where ζ is the distance from the source center, which moves with the flow. The amplitude A_E is the following function of time:

$$\frac{2A_E}{A_{\max}} = \begin{cases} 1 - \cos\left(\frac{\pi t}{\tau_{\text{start}}}\right) \text{ if } 0 \le t \le \tau_{\text{start}} \\ 2 \text{ if } \tau_{\text{start}} < t \le \tau_{\text{start}} + \tau_{\max} \\ 1 + \cos\left(\frac{\pi(t-(\tau_{\text{start}}+\tau_{\max}))}{\tau_{\text{end}}}\right) \text{ if } \tau_{\text{start}} + \tau_{\max} < t \le \tau_{\text{start}} + \tau_{\max} + \tau_{\text{end}} \\ 0 \text{ for } \tau_{\text{start}} + \tau_{\max} + \tau_{\text{end}} < t < t_{\text{end}} \end{cases} \tag{33}$$

where the following parameters were user-set:

- $A_{\max}$, the maximum amplitude.
- τ_{start}, the lapse of time during which generation is initiated and smoothly ramped up.
- $\tau_{\max}$, the lapse of time during which entropy-patch generation is done with the maximum global amplitude.
- τ_{end}, the time during which the generation process is smoothly ramped down.
- t_{end}, the time at which entropy-patch generation ends.

I.e., entropy-patch generation comprises three phases, each of duration: τ_{start}, $\tau_{\max}$ and τ_{end}.

IV. Numerical-simulation results and comparison to theory

In Fig. 9, the upstream acoustic response p', scaled by the quasi-steady-model prediction (Eq. (5)), is plotted as a function of time. To calculate the quasi-steady-model prediction: the relative excess density $(\rho_e/\bar{\rho})$ was approximated by its amplitude $|\rho_e/\bar{\rho}|_{\max}$. Given that the entropy patches, which were generated, had negative excess density:

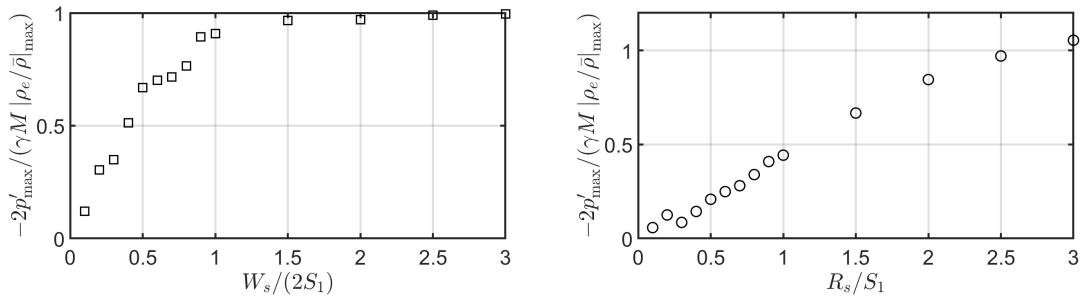

(a) Entropy slug (b) Entropy spot

Fig. 10 The upstream acoustic response amplitude vs. the entropy patch's normalized characteristic length.

$(\rho_e/\bar{\rho}) \simeq -|\rho_e/\bar{\rho}|_{\max}$ was used. Moreover, in Fig. 9: results obtained with two entropy-patch shapes—viz., an entropy slug (solid line) and spot (dashed line)—are compared. The results shown in Fig. 9(a) were obtained with $W_s/(2S_1) = 3.0$ (Fig. 8(c)) and $R_s/S_1 = 3.0$ ((Fig. 8(d))). Whereas the results in Figs. 9(b) where acquired $W_s/(2S_1) = 1.0$ (Fig. 8(a)) and $R_s/S_1 = 1.0$ ((Fig. 8(b))). One observes that for $R_s/S_1 = W_s/(2S_1) = 3.0$ and $W_s/(2S_1) = 1.0$ the quasi-steady model yields: a remarkably good prediction (especially for $W_s/(2S_1) = 3.0$) for the amplitude $p'_{\max}$, which is the local extremum in p'.

That said, in Fig. 9(b), one observes a marked deviation from the quasi-steady-model prediction for the $R_s/S_1 = 1.0$ case. What's more, in Fig. 9(a), one observes a slight deviation of ca. 5%, between the quasi-steady-model predictions for the slug and the spot, respectively. The authors note that the quasi-steady model is also quasi-1D in nature (§II.A), to wit, it cannot capture the effect of even subtle rounding of an entropy patch's edges. This leads the authors to reason that the shape and the size of the entropy patch: affect sound production due to entropy-patch-nozzle interaction.

To confirm the authors' reasoning: a series of cetris paribus simulations were carried out with various entropy-slug and -spot sizes; viz., R_s/S_1 and $W_s/(2S_1)$ were varied. The results are shown in Figs. 10(a) and 10(b) for entropy slugs and spots, respectively. From data in Fig. 10 one gleans: quasi-steady modeling clearly captures the essence of sound production due to entropy patch nozzle interaction—provided that the characteristic length of the patch L_s, be it R_s or W_s, is about the same as or larger than the upstream-channel height. Ergo, in the case of a choked-nozzle flow for which $L_s/S_1 \gtrsim 2$: entropy-patch-nozzle interaction is dominated by quasi-steady effects—going forward, this will be referred to as the quasi-steady-modeling regime.

For $L_s/S_1 \lesssim 2$, the data in Fig. 10, indicate that quasi-steady effects no longer dominate. With that in mind, the authors reasoned that outside of said quasi-steady-modeling regime: inertial effects start to play a non-negligible role. Moreover, the authors hypothesized that there is an inertial-modeling regime. To wit, a regime where acceleration of the entropy patch through the choked nozzle plays an essential role in the establishment of the upstream acoustic response. Furthermore, the authors reasoned that the said inertial regime would be most likely be attained when one considers

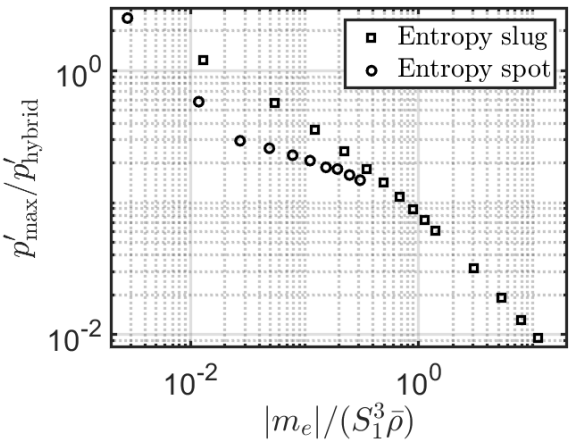

Fig. 11 Comparison of the simulation's upstream acoustic-response amplitude $p'_{\max}$ to the associated hybrid-model predictions p'_{hybrid} vs. the estimated excess mass $|m_e|$ carried by the entropy patch.

entropy patches of very small extent. In other words, the authors reasoned that if the entropy patch is quite small—viz., point-particle like or in Ffowcs-Williams & Howe's words: a "pellet"—the establishment of an upstream acoustic response would be dominated by inertial effects. In particular, the authors reasoned that in said inertial-modeling regime: convective acceleration would be the most consequential modeling ingredient.

To test the authors' hypothesis re the existence of an inertial-modeling regime: the simulation results were compared to the quasi-one-dimensional point-mass model (or the hybrid model) proposed in §II.B. To do so the authors needed to estimate the excess mass m_e carried by the entropy patch—the reader is referred to appendix B for more information on how this was done—in an unsteady entropy-patch-nozzle simulation.

In Fig. 11, the simulation's upstream acoustic-response amplitude $p'_{\max}$ is compared to its associated hybrid-model prediction p'_{hybrid}. In particular, $p'_{\max}/p'_{\text{hybrid}}$ is shown as a function of the estimated excess mass $|m_e|/(S_1^3\bar{\rho})$ carried by the entropy patch.

One observes that as $|m_e|$ becomes smaller—i.e., the size of the patch becomes smaller—$p'_{\max}/p'_{\text{hybrid}}$ becomes order one; viz., $p'_{\max}/p_{\text{hybrid}} = \mathrm{O}(1)$. This indicates, in the authors' view, that there is indeed an inertial regime, and that it is reached, when: sufficiently small entropy patches—i.e., for spots $|m_e|/(S_1^3\bar{\rho}) \lesssim 10^{-2}$, which corresponds to $R_s/S_1 = 0.2$ & for slugs $|m_e|/(S_1^3\bar{\rho}) \lesssim 5 \times 10^{-2}$, which corresponds $W_s/(2S_1) = 0.2$—engender the upstream acoustic response as they are ingested by the choked nozzle.

The corollary to the data reflecting the existence of two clearly-distinct modeling regimes— viz., an inertial-modeling regime for small enough entropy patches ($L_s/S_1 \lesssim 0.2$) and a quasi-steady-modeling regime for large enough patches ($L_s/S_1 \gtrsim 2$)—is, that there is a regime between the aforementioned two regimes. Moreover, the authors posit: in said connecting regime a blend of quasi-steady and inertial effects play a role in the generation of an upstream acoustic response due to entropy-patch-nozzle interaction. Going forward, this posited regime will be referred to as: the

blended-physical-effects regime.

This leads the authors to conclude: in the case of entropy-patch choked-nozzle interaction size and shape do matter.

V. Conclusion

Analysis of dedicated numerical simulations presented in this paper shows that, in the case choked-nozzle flows when the characteristic length of the entropy patch L_s is roughly the same as or larger than the upstream channel height: sound production due to entropy-patch-nozzle interaction is clearly dominated by quasi-steady effects. Ergo, if $L_s/S_1 \gtrsim 2$ entropy-patch-nozzle interaction is said to be in the quasi-steady-modeling regime. Sound production due to the passage of two types of entropy patches moving through a nozzle atop a steady-choked-nozzle flow were investigated; viz., rectangular slugs and circular spots. All the slugs had a height equal to that of the channel upstream from the choked nozzle. In both cases, the size of the patches was varied by changing its characteristic length, to wit, the width of the slug W_s or the radius of the spot R_s. The presented analysis indicates that for small enough entropy patches, $L_s/S_1 \lesssim 0.2$, inertial effects govern the production of the upstream acoustic response. The authors propose that this regime be referred to as the inertial-modeling regime. In addition, the data reflect that the aforementioned regimes are clearly-distinct. Ergo, the authors posit: there is a regime between said two regimes, which they move be called: the blended-physical-effects regime. In the later regime, the authors hypothesize: a blend of quasi-steady and inertial effects play a role in the generation of an upstream acoustic response due to entropy-patch-nozzle interaction.

A. Hybrid point-mass model: convective acceleration estimation

As was alluded to in section II.B, one can estimate the convective acceleration term $u\mathrm{d}u/\mathrm{d}x$ in Eq. (23) from the stationary base flow simulation result. To do this the Paraview functions "plot over line" and "spreadsheet view" were used to extract the velocity data along the line between points $(x_{\text{in}}, 0.99S_1)$ and $(x_{\text{th}}, 0.99S_1)$ as sketched in Fig. 12. The extraction line is sketched in Fig. 12 as a black arrow in the streamwise direction. The spatial coordinates and velocity data are exported as comma separated value files using the "export spreadsheet" functionality in Paraview's "spreadsheet view." The values were extracted form a hundred equidistant points each separated by a distance ΔX. The data were loaded into Matlab with the "readscv" function, and two arrays $\mathbf{X}$ and $\mathbf{U}$ with horizontal coordinates and velocity were defined. The convective acceleration array $\mathbf{A}_c$ was then estimated, as follows:

$$A_{c,i} = U_i \frac{U_i - U_{i-1}}{\Delta X} \tag{34}$$

where the subscript i represent the i^{th} array element.

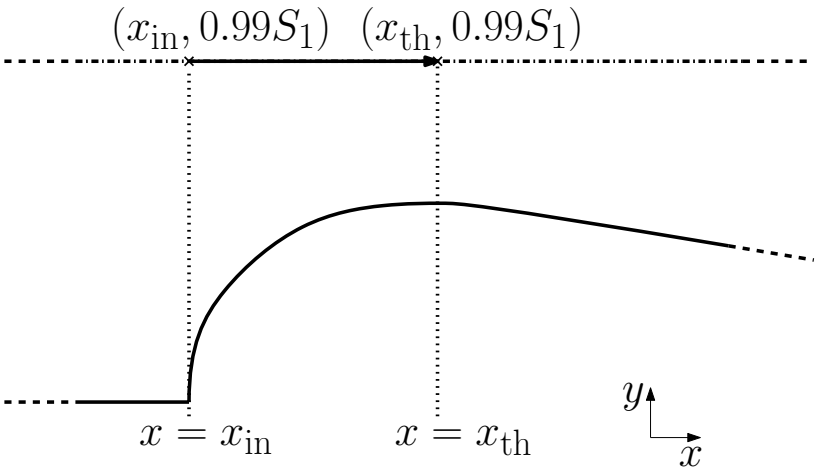

Fig. 12 Sketch of line over which coordinates and velocity data were extracted with Paraview.

B. Excess-mass estimation

In this appendix an estimation of the the excess mass m_e carried by the entropy patch is provided. Said excess mass defined, as follows:

$$m_e \equiv \int_{V_e} \rho_e \mathrm{d}^3 x \tag{35}$$

in §B.A and §B.B this a relation used to estimate m_e for circular spots and rectangular slug are derived, respectively.

A. Excess mass circular spot

Based on the density distribution in a mature spot, it is the authors judgment that a Gaussian distribution for ρ_e can be assumed. Thus, one has:

$$\rho_e = \rho_{e,\text{ext}} \exp\left(-\frac{x^2 + y^2}{R_s^2}\right) = \rho_{e,\text{ext}} \exp\left(-\frac{r^2}{R_s^2}\right) \tag{36}$$

Defining the upstream-channel width $W_c = S_1$. Moreover, assuming an unbounded space—i.e., not taking into account spots with a radius larger than half the upstream-channel height. One can estimate the excess mass in a circular spot, as follows:

$$m_e \simeq W_c \int_{-\infty}^{\infty} \int_{-\infty}^{\infty} \rho_e \mathrm{d}x\mathrm{d}y \tag{37}$$

which can obviously be rewritten as

$$m_e \simeq W_c \int_{0}^{\infty} \rho_e 2\pi r \mathrm{d}r \tag{38}$$

Substituting Eq. 36, one finds:

$$m_e \simeq W_c \rho_{e,\text{ext}} \int_0^\infty \exp\left(-\frac{r^2}{R_s^2}\right) 2\pi r \mathrm{d}r \tag{39}$$

$$= W_c \rho_{e,\text{ext}} \pi R_s^2 \int_0^\infty \exp\left(-\frac{r^2}{R_s^2}\right) \mathrm{d}\left(\frac{r^2}{R_s^2}\right) \tag{40}$$

which yields

$$m_e \simeq W_c \rho_{e,\text{ext}} \pi R_s^2 = S_1 \rho_{e,\text{ext}} \pi R_s^2 \tag{41}$$

B. Excess mass rectangular slug

Based on the density distribution in a mature slug, it is the authors judgment that a Gaussian distribution for ρ_e can be assumed. Ergo, one has:

$$\rho_e = \rho_{e,\text{ext}} \exp\left(-\frac{x^2}{(W_s/2)^2}\right) \tag{42}$$

Taking upstream-channel height $H_c = 2S_1$ and its width is $W_c = S_1$, the excess mass can be estimated as follows:

$$m_e \simeq W_c H_c \int_{-\infty}^\infty \rho_e \mathrm{d}x \tag{43}$$

$$= W_c H_c \rho_{e,\text{ext}} \int_{-\infty}^\infty \exp\left(-\frac{x^2}{(W_s/2)^2}\right) \mathrm{d}x \tag{44}$$

$$= W_c H_c \rho_{e,\text{ext}} I_{\text{int}} \tag{45}$$

where

$$I_{\text{int}} = \int_{-\infty}^\infty \exp\left(\frac{x^2}{(W_s/2)^2}\right) \mathrm{d}x \tag{46}$$

Taking the square of I_{int}, one has

$$
\begin{aligned}
I_{\text{int}}^2 &= \int_{-\infty}^{\infty} \exp\left(-\frac{x^2}{(W_s/2)^2}\right) \mathrm{d}x \\
&= \int_{-\infty}^{\infty} \exp\left(-\frac{x^2}{(W_s/2)^2}\right) \mathrm{d}x \int_{-\infty}^{\infty} \exp\left(-\frac{y^2}{(W_s/2)^2}\right) \mathrm{d}y \\
&= \int_{-\infty}^{\infty}\int_{-\infty}^{\infty} \exp\left(-\frac{x^2+y^2}{(W_s/2)^2}\right) \mathrm{d}x\mathrm{d}y \\
&= \int_{0}^{\infty} \exp\left(-\frac{r^2}{(W_s/2)^2}\right) 2\pi \mathrm{d}r = \pi\left(\frac{W_s}{2}\right)^2
\end{aligned} \tag{47}
$$

Taking the square-root of this result, yields:

$$
I_{\text{int}} = \sqrt{\pi}\left(\frac{W_s}{2}\right) \tag{48}
$$

Substituting this result in Eq. (45), one finds:

$$
m_e \simeq W_c H_c \sqrt{\pi}\left(\frac{W_s}{2}\right)\rho_{e,\text{ext}} = S_1^2 \sqrt{\pi} W_s \rho_{e,\text{ext}} \tag{49}
$$

Acknowledgments

Kurt Kowalski expresses his gratitude for the support offered by the Engineering Fluid Dynamics group (chaired by Kees Venner) both in terms of: academic supervision & the covered 30th AIAA/CEAS attendance fee. The authors thank Avraham Hirschberg for the thoughtful & meaningful conversations about the presently-reported work. Lionel Hirschberg thanks Catherine Lemaitre and Assa Ashuach for their help.

References

[1] Strahle, W. C., "On combustion generated noise," *Journal of Fluid Mechanics*, Vol. 49, No. 2, 1971, pp. 399–414. doi: 10.1017/S0022112071002167.

[2] Dowling, A. P., and Mahmoudi, Y., "Combustion Noise," *Proceedings of the Combustion Institute*, Vol. 35, No. 1, 2015, pp. 65–100. doi:10.1016/j.proci.2014.08.016.

[3] Morgans, A. S., and Duran, I., "Entropy Noise: A Review of Theory, Progress and Challenges," *International Journal of Spray and Combustion Dynamics*, Vol. 8, No. 4, 2016, pp. 285–298. doi:10.1177/1756827716651791.

[4] Dotson, K. W., Koshigoe, S., and Pace, K. K., "Vortex Shedding in a Large Solid Rocket Motor Without Inhibitors at the Segmented Interfaces," *Journal of Propulsion and Power*, Vol. 13, No. 2, 1997, pp. 197–206. doi:10.2514/2.5170.

[5] Hulshoff, S. J., Hirschberg, A., and Hofmans, G. C. J., "Sound production of vortex nozzle interactions," *Journal of Fluid Mechanics*, Vol. 439, 2001, pp. 335–352. doi:10.1017/S0022112001004554.

[6] Anthoine, J., Buchlin, J.-M., and Hirschberg, A., "Effect of Nozzle Cavity on Resonance in Large SRM: Theoretical Modeling," *Journal of Propulsion and Power*, Vol. 18, No. 2, 2002, pp. 304–311. doi:10.2514/2.5935.

[7] Hirschberg, L., Hulshoff, S. J., Collinet, J., Schram, C., and Schuller, T., "Vortex nozzle interaction in solid rocket motors: A scaling law for upstream acoustic response," *Journal of the Acoustical Society of America*, Vol. 144, No. 1, 2018, pp. EL46–EL51. doi:10.1121/1.5046441.

[8] Hirschberg, L., Hulshoff, S. J., Collinet, J., Schram, C., and Schuller, T., "Influence of Nozzle Cavity on Indirect Vortex- and Entropy-Sound Production," *AIAA Journal*, Vol. 57, No. 7, 2019, pp. 3100–3103. doi:10.2514/1.J058138.

[9] Hirschberg, L., and Hulshoff, S. J., "Lumped-Element Model for Vortex-Nozzle Interaction in Solid Rocket Motors," *AIAA Journal*, Vol. 58, No. 7, 2020, pp. 3241–3244. doi:10.2514/1.J058673.

[10] Bake, F., Richter, C., Muhlbauer, B., Kings, N., Rohle, I., Thiele, F., and Noll, B., "The Entropy-Wave Generator (EWG): A reference case on entropy noise," *Journal of Sound and Vibration*, 2009, pp. 574–598. doi:10.1016/j.jsv.2009.05.018.

[11] Kings, N., and Bake, F., "Indirect combustion noise: noise generation by accelerated vorticity in a nozzle flow," *International Journal of Spray and Combustion Dynamics*, Vol. 2, No. 3, 2010, pp. 253–266. doi:10.1260/1756-8277.2.3.253.

[12] Kings, N., "Indirect combustion noise: Experimental investigation of the vortex sound generation in nozzle flows," Ph.D. thesis, Technische Universität Berlin, 2015.

[13] Hirschberg, L., Bake, F., Knobloch, K., and Hulshoff, S. J., "Swirl-Nozzle Interaction Experiments: Influence of Injection-Reservoir Pressure and Injection Time," *AIAA Journal*, Vol. 59, No. 7, 2021, pp. 2806–2810. doi:10.2514/1.J060291.

[14] De Domenico, F., Rolland, E., Rodrigues, J., Magri, L., and Hochgreb, S., "Compositional and entropy indirect noise generated in subsonic non-isentropic nozzles," *Journal of Fluid Mechanics*, Vol. 910, 2021, pp. A5 1–31. doi:10.1017/jfm.2020.916.

[15] Wellemann, M., and Noiray, N., "Experiments on sound reflection and production by choked nozzle flows subject to acoustic and entropy waves," *Journal of Sound and Vibration*, Vol. 492, 2021, p. 115799. doi:10.1016/j.jsv.2020.115799.

[16] Hirschberg, L., Bake, F., Knobloch, K., Rudolphi, A., Kruck, S., Klose, O., and Hulshoff, S. J., "Swirl-Nozzle Interaction Experiment: Quasi-Steady Model Based Analysis," *Experiments in Fluids*, Vol. 62, No. 175, 2021, pp. 1–16. doi:10.1007/s00348-021-03271-y.

[17] Hirschberg, L., Bake, F., Knobloch, K., Hulshoff, S., and Hirschberg, A., "Experimental investigations of indirect noise due to modulation of axial vorticity and entropy upstream of a choked nozzle," *Journal of sound and vibration*, Vol. 532, 2022. doi:10.1016/j.jsv.2022.116989.

[18] Marble, F. E., and Candel, S. M., "coustic disturbance from gas non-uniformities convected through a nozzle," *Journal of Sound and Vibration*, Vol. 55, 1977, pp. 225–243. doi:10.1016/0022-460X(77)90596-X.

[19] Ffowcs Williams, J. E., and Howe, M. S., "The generation of sound by density inhomogeneities in low Mach number nozzle flows," *Journal of Fluid Mechanics*, Vol. 70, No. 3, 1975, pp. 605–622. doi:10.1017/S0022112075002224.

[20] Leyko, M., Moreau, S., Nicoud, F., and Poinsot, T., "Numerical and analytical modelling of entropy noise in a supersonic nozzle with a shock," *Journal of Sound and Vibration*, Vol. 330, No. 16, 2011, pp. 3944–3958. doi:https://doi.org/10.1016/j.jsv.2011.01.025.

[21] Gentil, Y., Daviller, G., Moreau, S., and Poinsot, T., "Multispecies flow indirect-noise modeling re-examined with a helicopter-engine application," *AIAA Journal*, 2024, pp. 1–14. doi:10.2514/1.J063328.

[22] Curle, N., "The influence of solid boundaries upon aerodynamic sound," *Proc. Roy. Soc. A*, Vol. 231, 1955, pp. 505–514. doi:https://doi.org/10.1098/rspa.1955.0191.

[23] Pierce, A. D., *Acoustics: an introduction to its physical principles and applications*, Acoustical Society of America, Melville, New York, USA, 1994.

[24] Hulshoff, S. J., *EIA an Euler Code for Internal Aeroacoustics: method description and user's guide*, Faculty of Aerospace Engineering, Delft University of Technology, Delft, the Netherlands, October 2016.

[25] Hulshoff, S. J., Hirschberg, A., and Hofmans, G. C. J., "Sound production of vortex nozzle interaction," *Journal of Fluid Mechanics*, Vol. 439, 2001, pp. 335–352.

[26] Hirschberg, L., Hulshoff, S. J., Schuller, T., Schram, C. F., and Collinet, J., *Numerical simulations based evidence of impingement free sound production during vortex-nozzle interaction in solid rocket motors*, AIAA, 2019. doi:10.2514/6.2019-2421, URL https://arc.aiaa.org/doi/abs/10.2514/6.2019-2421.

[27] Hirschberg, L., "Low order modeling of vortex driven self-sustained pressure pulsations in solid rocket motors," Ph.D. thesis, CentraleSupélec, Université Paris-Sacly, 2019.

[28] Henrici, P., *Applied and Computational Complex Analysis*, Vol. I, Wiley-Interscience, NY, USA, 1974.

[29] Hirschberg, L., Schuller, T., Schram, C., Collinet, J., Yiao, M., and Hirschberg, A., "Interaction of a vortex with a contraction in a 2-dimensional channel: incompressible flow prediction of sound pulse," *23rd AIAA/CEAS Aeroacoustics conference*, 2017.

[30] Venkatakrishnan, V., and Jameson, A., "Computation of unsteady transonic flows by the solution of Euler equations," *AIAA Journal*, Vol. 26, No. 8, 1988, pp. 974–981.

[31] Hulshoff, S. J., *Computational modelling: lecture notes*, TU Delft, 2016.

[32] Thompson, P. A., *Compressible-Fluid Dynamics*, MacGraw Hill, NY, USA, 1972.